

Projection Welding with Pneumatic and Servomechanical Electrode Operating Force Systems

This research achieved an improvement in projection welding

BY Z. MIKNO

ABSTRACT

This article contains an analysis of the effect of two electrode force systems (pneumatic and servomechanical) on the formation of a projection weld. Calculations and experiments were conducted on steel DX53 (a 1.5-mm-thick test plate with an embossed projection) and for various values of electrode force (pneumatic system) and electrode travel (servomechanical system). The comparative analysis of the systems was performed using finite element method (FEM) calculations (SORPAS® software) and experimental verification. The research also involved destructive and nondestructive examinations (peeling and static tensile tests, plus metallographic examinations). The analysis included the space distribution of volumetric power density in the projection material to determine the heating efficiency of both electrode force systems. The presented method of force and travel of electrodes during projection welding was entirely different from methods used previously and changed the existing views on projection welding. The new solution consisted of applying a hybrid servomechanical force system for controlling both electrode force and electrode travel (force is controlled before and after the flow of current, whereas travel is controlled during the flow of current). The force applied before the flow of welding current was lower than the force exerted by the classical i.e., pneumatic force system. The main advantages of this solution were the following: 1) a smaller cold projection height reduction, 2) a smaller area of contact between materials being welded, and 3) melting of the projection material was initiated in the projection cap. All these three advantages enable the prevention of the formation of an undesirable ring weld at the beginning of a welding process. This solution makes it possible to extend a projection height reduction time (several times) and generate greater energy in the projection during the projection height reduction.

KEYWORDS

- Embossed Projection Welding • FEM Calculations • Resistance Welding
- Pneumatic Operating Force System • Servomechanical Operating Force System
- Electrode Movement Control

Introduction

Resistance welding has been known for more than 139 years (since 1877 with the first resistance welded joint) and remained to be a popular technology for joining thin-walled metal elements (mainly in the automotive industry) due to the following three ba-

sic and competitive advantages: 1) in most applications, there is no need to use filler metals, 2) the process of welding is fast (a short welding current flow time of ~200 ms), and 3) a low cost of welded joint production (~0.1 U.S. cent) (Ref. 1). Please note the data are concerned with the overlap welding of car body sheets having a thickness of ~1.0 mm.

For the reasons mentioned, resistance welding is the main joining technology in the automotive industry, even though alternative methods for the joining of car elements (including adhesive bonding, riveting, or laser welding) are available.

Depending on a model, it is estimated the production of a vehicle requires between 3000 and 5000 (or even more) welds. Welding is used for joining elements of critical importance, which, if joined improperly, may cause failures leading to significant material losses or situations dangerous to health and life.

These several thousand car body welds contain approximately 300 welded and clamped connectors, e.g., bolts, nuts, and pins. Key elements are fixed to, for instance, seat belts or steering columns and provide grounding for electric circuits. The quality of welded joints is critical as regards to safety and reliability (Ref. 2).

Electrode force is one of the three primary parameters of the welding process. The other two parameters are the value of current and time of current flow. During projection welding, in a conventional application, such as with a pneumatic force system, the parameter of electrode force is characterized by significant limitations. Due to its high inertia, pneumatic force cannot be applied whenever fast changes of force are required. For this reason, the value of preset force is usually constant and higher than required. It cannot be excessively high as it could cause a decrease in the height of a pro-

Z. MIKNO (zygmunt.mikno@is.gliwice.pl) is with the Department of Electronic Welding Devices, Welding Institute, Gliwice, Poland.

jection. It cannot be overly low as it is necessary to prevent liquid metal expulsion.

An alternative solution requires another method for exerting force on materials being welded (Refs. 3–6). In the pneumatic system, electrode force applied during welding results from a specific force value preset in a pneumatic cylinder. The travel of electrodes is the consequence of the effect of this force and the changeable mechanical resistance of the materials being welded. In the solution involving the servomechanical force system, the travel of electrodes is preset, and the resultant force depends on the travel of electrodes and resistance to deformation (the reduction of the height) of a projection being heated. Proper electrode force is required to ensure good contact between the electrodes and elements being welded; otherwise, it would be impossible to provide the flow of high welding current (reaching even tens of kA).

The purpose of this research was to obtain knowledge about the formation of a projection weld as regard to the conventional force system (pneumatic). The determination of mutual relationships between electrode force, intensity of the welding current, density of the welding current, and changing contact surface of a projection could make it possible to define the optimum trajectory and rate of electrode travel for the servomechanical system.

Present State

Many factors influence heat generated in the welding area and reduction of a projection height. The authors (Refs. 6, 7) state that the most important projection welding variables are the quality of projections (repeatability) and a cylinder reaction to a projection height reduction during welding. It was also assumed a pneumatic cylinder movement should adequately follow a projection height reduction. Unfortunately, often projection heating was observed outside the projection cap (Ref. 7). This causes the fast reduction of projection height during the flow of welding current without obtaining of a proper joint.

Reference 8 presents the influence of such factors as welding current and electrode force as well as the properties of

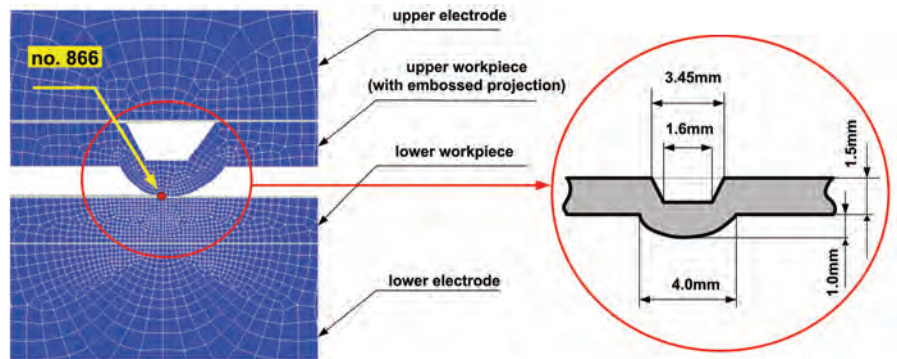


Fig. 1 — Computational model, projection dimensions, and location of points (nods) for the analysis of parameters.

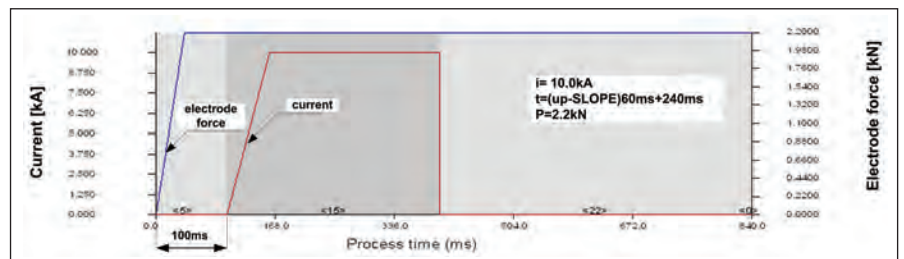


Fig. 2 — Computational program applied for projection welding with a pneumatic force system. The adopted parameters were as follows: current 10 kA, welding time 60 ms (upslope) + 240 ms, and electrode force (2.2 kN).

Table 1 — Simulation Parameters

	Squeeze	Upslope	Weld	Hold	
Time step increment					
Pneumatic force system	100	60	240	100	[ms]
Servomechanical force system	100	120	210	100	
Save data per	10	5	5	10	Steps
Coverage Control					
Electrical model					Covergence Accuracy
Thermal model					1.00E-5
Mechanical model					1.00E-5
Dynamic contact between materials					Sliding
Heat loss to surroundings					
Air temperature					20 °C
Heat transfer rate					300 [W/m ² *K]
Electrode diameter					30 [mm]
Electrode height					20 [mm]
Welding current					DC

welded materials tested by the means of numerical methods. It was observed the surface of contact depends on the reduction of a projection height and of key importance at the initial heating time of projection welding. In such conditions (primarily due to the use of the pneumatic force system and necessary-

but excessively high force exerted by it), a ring weld nugget was formed on the perimeter. Such a formation was often accompanied by liquid metal expulsion. It should be noted the formation of an undesirable ring weld results from the previously mentioned excessively large and inconvenient (cold) projection

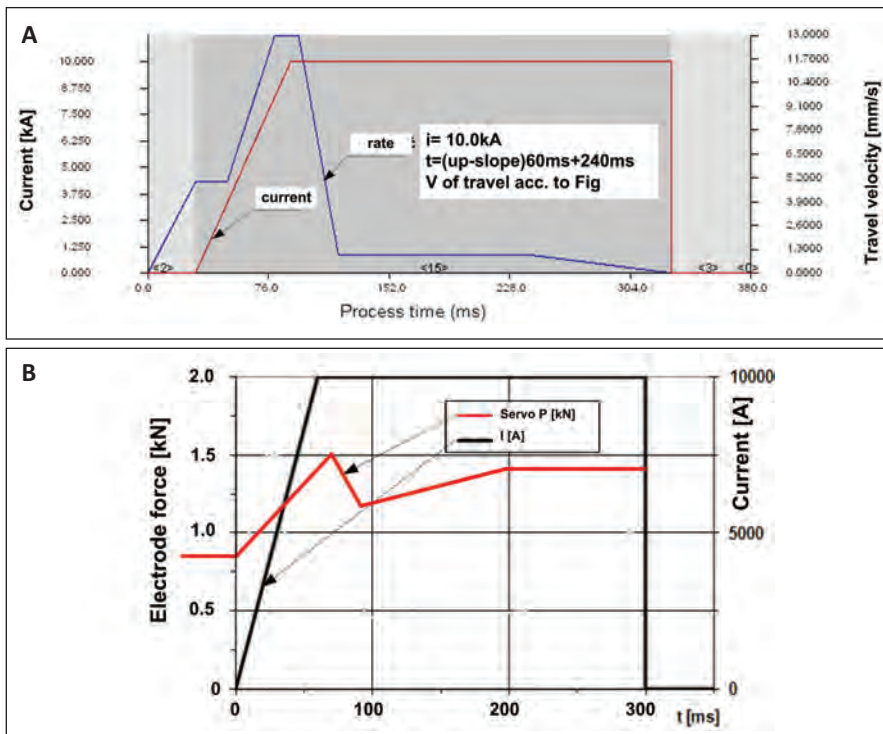


Fig. 3 — Computational program applied for projection welding with a servomechanical force system. The adopted parameters were as follows: current 10 kA, welding time 60 ms (upslope) + 240 ms. A — Electrode travel rate; B — resultant electrode force.

height reduction taking place before the flow of current. In turn, the significant reduction of projection height results from the use of excessively high force. The value of force results from the application of a pneumatic force system integrated with a welding machine.

In the study (Ref. 9), the process of projection welding was widely tested using numerical calculations. It was observed high welding parameters (high force, high value of current, and short time of current flow) were more favorable. However, this translated into an increasingly short welding time. This observation could imply capacitor welding would be the best solution. However, Reference 10 stated that in capacitor welding, due to a short current flow time, it was necessary to ensure a high rate of a force change. Moreover, the window of welding parameters was narrow. An increase in charging voltage (greater energy) increased a weld nugget area, yet required higher force. As a result, the issue remained unsolved.

The situation seems insoluble. It was not possible to infinitely increase

Table 2 — Material Properties of DX53 Steel (Ref. 16)

Temperature [°C]	Thermal Conductivity [W/m*K]	Temperature [°C]	Heat Capacity [J/kg*K]	Temperature [°C]	Resistivity [μΩ*m]	Temperature [°C]	Mass Density [kg/m ³]	Temperature [°C]	Thermal Expansion Coefficient [10 ⁻⁶ /°C]	Temperature [°C]	Young's Modulus of Elasticity [kN/mm ²]
20	65.1	20	481	20	0.117	20	7872	100	12.6	25	200
100	54.8	150	519	100	0.117			200	13.1		
200	52.1	200	536	200	0.236			300	13.5		
400	38.4	250	553	400	0.455			400	13.7		
600	30.2	300	574	600	0.752			500	14.2		
700	27.5	350	595	700	0.921			600	14.6		
900	27.0	450	662	900	1.13			700	14.9		
1100	30.3	550	754	1100	1.179			800	16.6		
1300	33.3	650	867	1300	1.229			1000	13.7		
1500	37.3	700	1139	1500	1.235						
		750	875								
		850	846								

Table 3 — Material Properties of Electrode Material A3/1 CuCoBe (ISO 5182) (Ref. 16)

Temperature [°C]	Thermal Conductivity [W/m*K]	Temperature [°C]	Heat Capacity [J/kg*K]	Temperature [°C]	Resistivity [μΩ*m]	Temperature [°C]	Mass Density [kg/m ³]	Temperature [°C]	Thermal Expansion Coefficient [10 ⁻⁶ /°C]	Temperature [°C]	Young's Modulus of Elasticity [kN/mm ²]
20	217.5	20	420	20	0.033	20	8750	25	16.5	25	117
100	246.6	127	446	100	0.037	927	529				
300	281.9	327	466	300	0.050						
500	305.6	527	482	500	0.062						
700	314.1	727	500	700	0.076						
900	316.0	927	529	900	0.091						

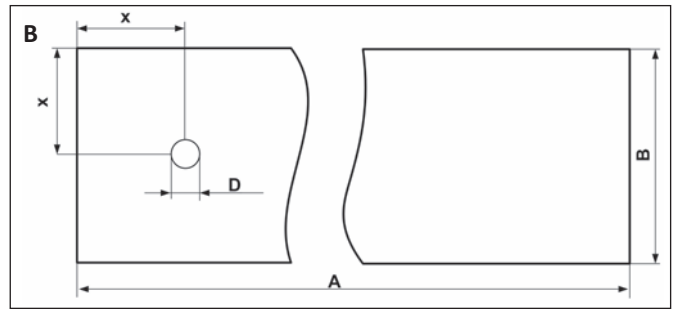
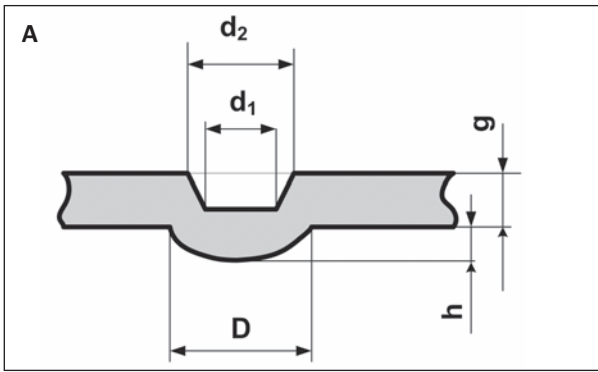


Fig. 4 — A — Projection; B — welded elements (sheets) dimensions.

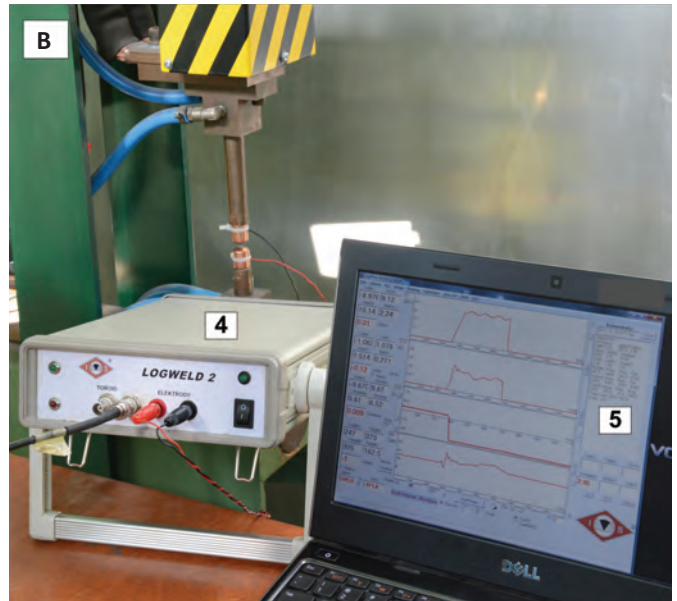


Fig. 5 — A — Testing station for resistance welding with a servo-mechanical electrode force system; B — measurement system. 1) welding machine housing, 2) servomotors, 3) control cabinet, 4) system LogWeld 2, and 5) computer.

the current and shorten the time of current flow as it would require the high dynamics (rate) of electrode force. In turn, the high dynamics of the force system entails the high value of force, which, in turn, leads to the undesirable (excessive) reduction of a

projection height. In addition, at an increasingly short welding time (the time of current flow), it is increasingly difficult to ensure proper (stable and repeatable) conditions ensuring the uniform heating (melting) of the projection (for ensuring the uniform re-

duction of a projection height and maintaining the constant density of current in the area of contact between the elements being welded (the projection)). Therefore, it can be stated there was a certain boundary above which high parameters cannot be used. The primary disadvantage of this boundary value was the necessity of the fast action of force.

In the pneumatic force system, an increase in force results in an increase in an electrode travel rate. However, the higher force reduces a projection height and, as a result, also reduces the resistance of contact, thus decreasing the density of current. Consequently, a smaller nugget size (as regards to its volume and diameter) was obtained.

The above analyses and observations related to projection welding were concerned with the pneumatic force

Table 4 — Projection and Sample Dimensions

Dimension	[mm]	Test Type
A	30	Metallographic Shear Testing
A	105	
B	30	
D	4.0	
X	15.0	
h	1.0	
g	1.5	
d_1	1.6	
d_2	3.45	

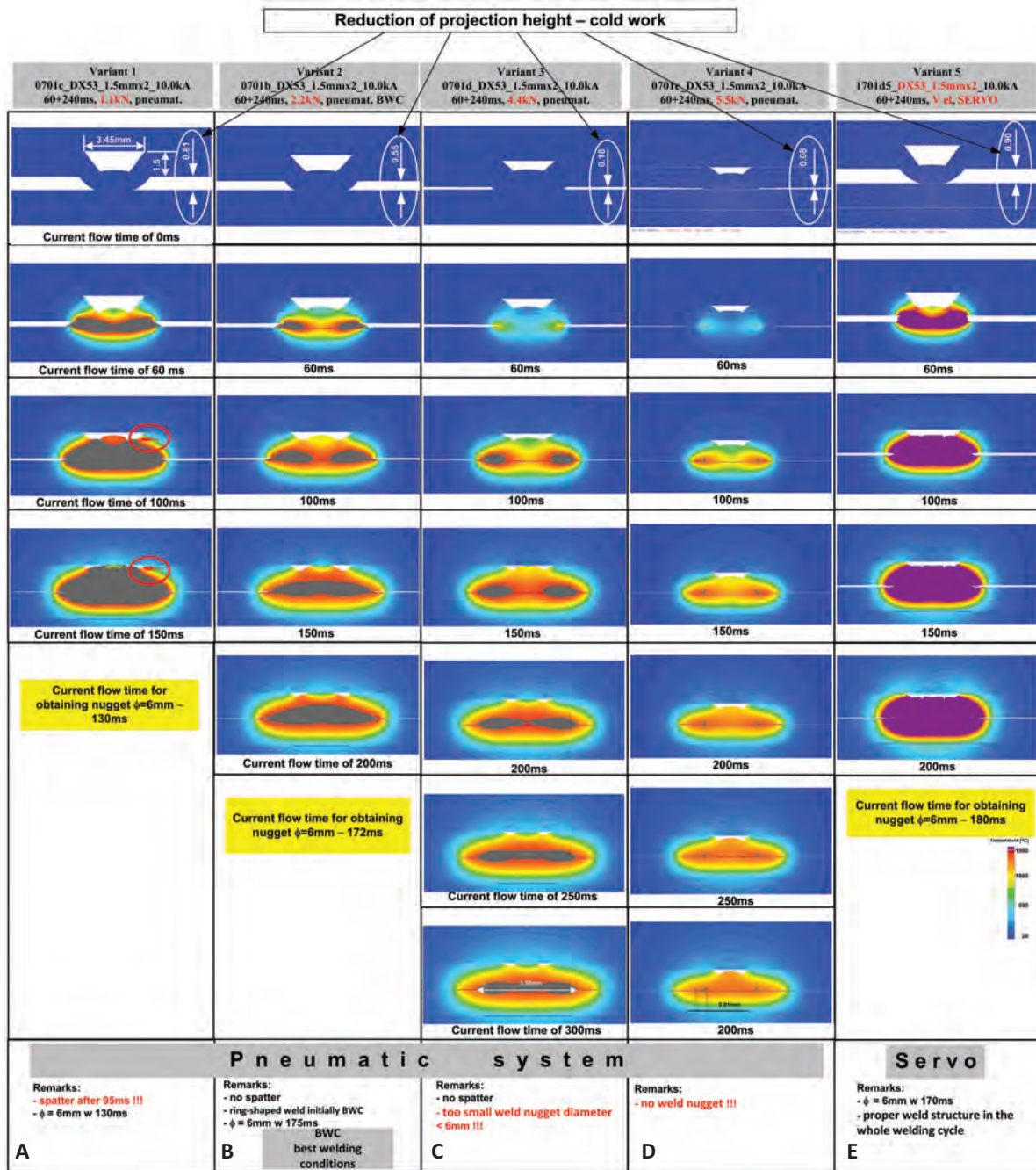


Fig. 6 – Formation of a projection joint along with the temperature distribution for selected times of welding current flow (0, 60, 100, 150, 200, 250, and 300 ms) with pneumatic (A, B, C, and D) and servomechanical force system (E). Welding current $i_{weld} = 10\text{ kA}$, welding time $t_{weld} = 60\text{ (upslope)} + 240\text{ ms}$, electrode force. A – 1.1 kN; B – 2.2 kN; C – 4.4 kN; D – 5.5 kN; and E – servomechanical force system.

Table 5 – Chemical Composition of Welded Material (DX53)

Steel Grade	C max	Mn max	P max	S max	Ti and/or NB max
DX 51 D – DX 57 D	0.12	0.60	0.045	0.045	0.30

system. To significantly change the course of a welding process (particularly the course of projection welding), it was necessary to use the servomechanical force system. In addition, the manner of electrode movement control, particularly during the flow of current, was of great importance.

Available reference publications do not contain information concerning

Calculation Model

The numerical model was developed for the case analyzed in the research, i.e., the welding of sheets with an embossed projection — Fig. 1.

Calculations related to the welding process concerned the analysis of dynamic resistance variability, momentary power of weld nugget expansion (of the weld nugget diameter and volume), and energy supplied to a weld. However, the primary purpose was to determine the most favorable welding power space distribution to obtain the desirable shape of the weld nugget not only at the end, but also during and, particularly, at the beginning of a welding process.

On the basis of related standards and instructions, the following projection type and welding parameters were assumed:

- 1) Current intensity, $i = 10.0$ kA, upslope (the time of an increase in current) 60 ms + main welding time 240 ms (Ref. 14).
- 2) Force, $F = 1.1 - 5.5$ kN for the pneumatic force system.
- 3) Travel control for the servomechanical electrode force system.
- 4) C-type projection (Refs. 14, 15) (the projection height is 1 mm, and the diameter of the projection base is 4 mm).

Figure 1 presents a projection welding computational model with characteristic points (for analysis), the mesh of elements, and projection dimensions for 1.5-mm-thick DX53 steel plates.

Simulation parameters used in this study for the FEM computational software are presented in Table 1.

Additional parameters and data necessary for performing numerical calculations being physical properties

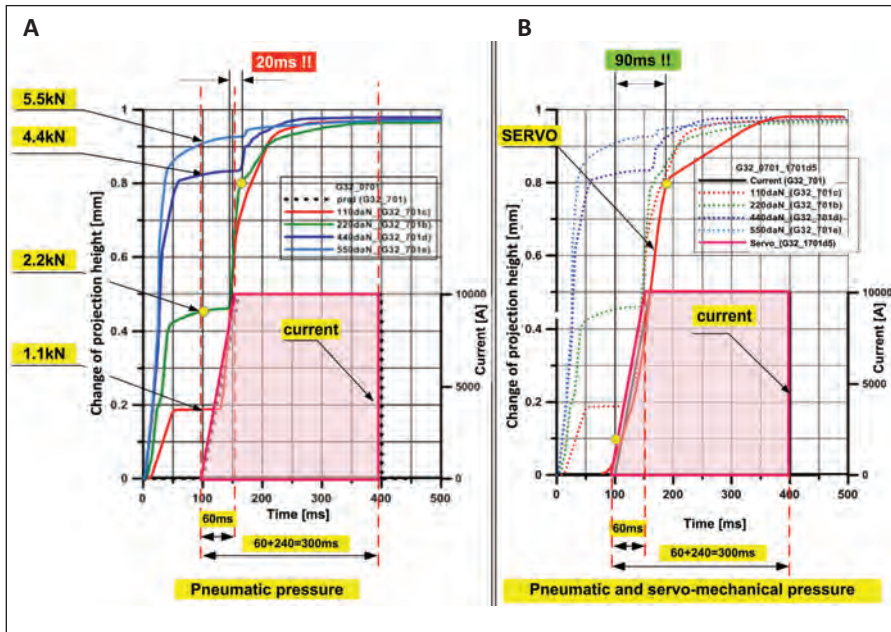


Fig. 7 — Change in the projection height during the welding time. A — Pneumatic system and the following parameters: initial force time $t_{init_force} = 100$ ms, welding current $i_{weld} = 10$ kA, welding time $t_{weld} = 60$ (upslope) + 240 ms, and electrode force 1.1/2.2/4.4 and 5.5 kN. B — Servomechanical system (solid line) and, for comparison with the pneumatic force system (dashed line), the same energy parameters (current and time).

such a method of electrode movement control as the one presented in this article (Ref. 11). References 11 and 12 propose an entirely different solution, including slowing down the travel of an electrode. In the author’s opinion, this approach was innovative and characterized by advantages worth mentioning. It was possible to extend the time of projection height reduction and generate more energy in the most desirable place, i.e., projection cap. The innovative electrode travel control significantly changes the previous approach to the course of a resistance welding process (particularly to projection welding) and significantly affects the development of the entire research area (pressure welding).

Numerical and Experimental Procedure

FEM Calculations

The research-related finite element method (FEM) calculations were conducted using version 11.2 of the SORPAS® software (Ref. 13). The software application enables carrying out associated analyses, including coupled electro-thermo-mechanical analyses.

This software features a module, including the effect of a new force solution and precise electrode movement solution, by the servomechanical system.

Table 6 — Parameters and Results for Pneumatic Electrode Operating Force System

No.	Upslope		Primary Welding Interval				E [kJ]		Projection Height Reduction Time [ms]	φ Nugget [mm]	Strength (Average) [kN]	Number of Tests	
	Force [kN]	Current [kA]	Time [ms]	Current [kA]	Time [ms]	I_{rms} [kA] (Total)	I_{rms} [kA] (PR)	Projection F1					Total F2
	A	B1	B2	C1	C2	D1	D2	G	J	K			
1	2.2	8.5	6.0	8.5	240	8.1	8.5	0.2	2.0	22	5.5	7.0	30
2	2.2	9.5	6.0	9.5	240	9.2	9.5	0.15	2.3	15	6.0	8.5	30

I_{rms} – Root-Mean-Square Current
PR – Primary Range

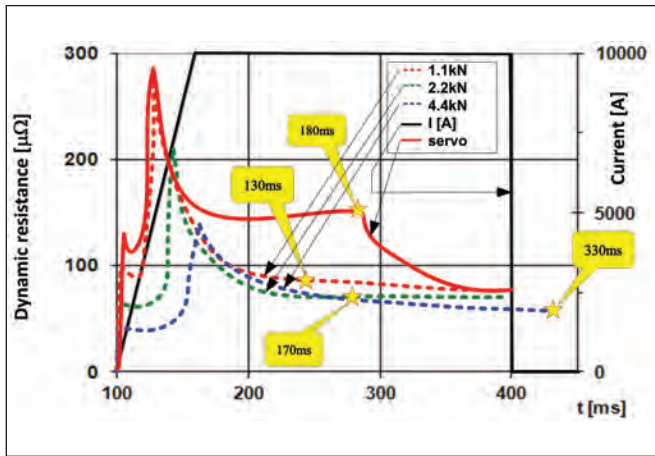


Fig. 8 — Course of dynamic resistance of projection welding for steel plates DX53 of thickness 1.5 + 1.5 mm, $i_{weld} = 10 \text{ kA}$, $t_{weld} = 60$ (upslope) + 240 ms for the pneumatic system and electrode force 1.1, 2.2, and 4.4 kN (dashed line), and the servomechanical electrode force system (solid line).

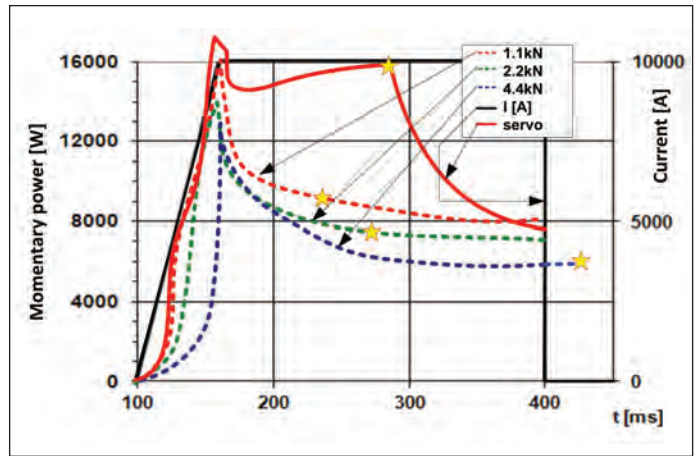


Fig. 9 — Course of momentary power of projection welding for steel plates DX53 of thickness 1.5 + 1.5 mm, $i_{weld} = 10 \text{ kA}$, $t_{weld} = 60$ (upslope) + 240 ms for the pneumatic electrode force system 1.1, 2.2, and 4.4 kN (dashed line), and the servomechanical electrode force system (solid line).

in the function of the temperature of a welded material and copper electrode are shown in Tables 2 and 3.

Process Parameters

The numerical welding calculation tests were conducted for the same current value (10.0 kA), same time of welding current flow (60-ms upslope) (increasing current), and the main welding current of 240 ms. The simulations for the pneumatic force system were conducted for four values of electrode force: $F = 1.1/2.2/4.4/5.5 \text{ kN}$ — Fig. 2 for $F = 2.2 \text{ kN}$. The boundaries of force values were 1.1 and 5.5 kN.

In regard to the servomechanical

force system, the exemplary electrode travel velocity and resultant electrode force are presented — Fig. 3. The parameters mentioned are associated with the most important process parameter, i.e., travel of the electrode.

The upslope of welding current was used to reduce (eliminate) the expulsion effect that was observed both in the numerical calculations and during the experimental tests without the upslope. The expulsion of a melted material was an undesirable effect causing shunting (Refs. 9, 12).

The dimension designations of the projection and welded materials are presented — Fig. 4. The values of the dimension designations of the projec-

tion and welded materials, shown in Fig. 4, are presented (Table 4).

Experimental Procedure

The research-related tests involved the use of steel DX53. The dimensions of the specimens used in the tests were 30 × 30 mm (for metallography) and 30 × 105 mm (for tensile shear tests). Before welding, the specimens were degreased using ethanol and a piece of flannel cloth. The chemical composition of the welded material is presented in Table 5.

The technological projection welding test was conducted using a model DC ($f = 1 \text{ kHz}$) inverter welding machine.

Table 7 — Parameters and Results for Servomechanical Operating Force System

No.	Force [kN]			Upslope		Main Welding Interval				Time and Movements of Electrodes [ms/mm]				Energy(kJ)		Projection Height Reduction Time (ms)	φ Nugget (mm)	Strength (average) (kN)	Number of Tests	
	Initial	Minimum	Maximum	Current (kA)	Time (ms)	Current (kA)	Time (ms)	I_{rms} [kA] (total)	I_{rms} (weld) [kA] (PR)	$t_1/\Delta t_1$	$t_2/\Delta t_2$	$t_3/\Delta t_3$	$t_4/\Delta t_4$	Projection Total	F2					
	A1	A2	A3	B1	B2	C1	C2	D1	D2	E1	E2	E3	E4	F1	F2	G	I	J	K	
1	40	70	150	8.5	120	8.5	210	8.3	8.5	60	30	30	210	0.55	2.2	120	6.0	7.5	30	
	—	—	—							/	/	/	/					—		
	50	90	180							0.05	0.5	0.4	0.25					8.0		
2	40	70	150	9.0	120	9.0	210	9.3	9.0	60	30	30	210	0.50	2.0	100	6.0	7.5	30	
	—	—	—							/	/	/	/					—		
	50	90	180							0.05	0.5	0.4	0.25					8.0		

I_{rms} —Root-Mean-Square Current

PR — Primary Range

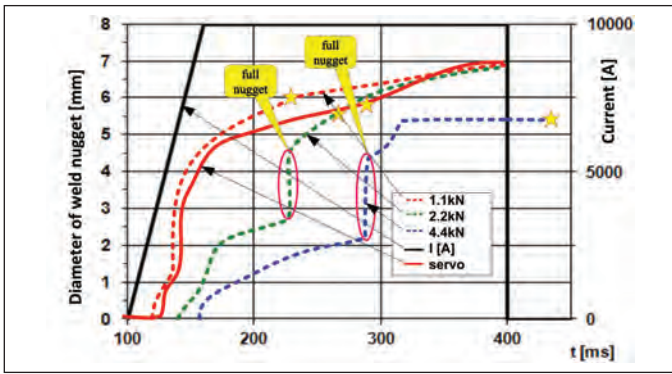


Fig. 10 — Simulation of weld nugget diameter growth for steel plates DX53 of thickness 1.5 + 1.5 mm, $i_{weld} = 10$ kA, $t_{weld} = 60$ (up-slope) + 240 ms for the pneumatic electrode force system 1.1, 2.2, and 4.4 kN (dashed line), and the servomechanical electrode force system (solid line).

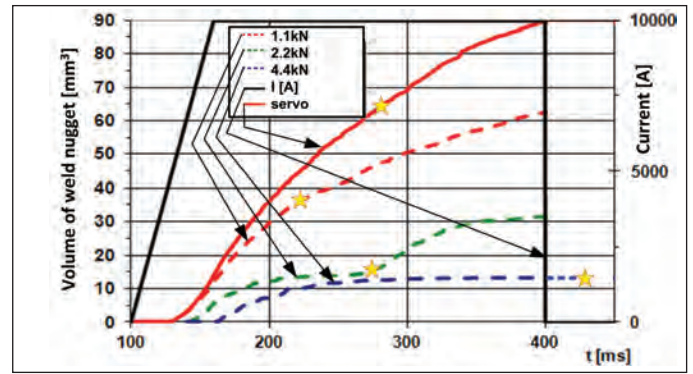


Fig. 11 — Simulation of weld nugget volume increase for steel plates DX53 of thickness 1.5 + 1.5 mm, $i_{weld} = 10$ kA, $t_{weld} = 60$ (up-slope) + 240 ms, and electrode force 1.1, 2.2, 4.4, and 5.5 kN.

Tests were carried out using the testing station shown in Fig. 5A. The experimental test performed using a welding machine included measurements of welding parameters, such as welding current and voltage, electrode travel (the reduction of a projection height), and electrode force. The parameters were measured with the LogWeld 2 special measurement device for resistance welding — Fig. 5B. This device can calculate additional parameters such as the waveform of momentary power, waveform of dynamic resistance, and energy supplied to the weld. The device also has many useful features used for the

analysis of recorded parameters (the present value or the value for a given period of time).

The preset welding parameters for the pneumatic force system are shown in Table 6 (columns with force, currents, and times for upslope and primary welding interval, I_{rms} [kA], and $I_{rms(weld)}$), whereas the preset welding parameters for the servomechanical force and/or travel system are shown in Table 7. They present the selected (exemplary) profiles of electrode travel.

It should be mentioned more profiles of this type are possible. In the case of the servomechanical system,

the travel of electrodes was determined experimentally for a given sheet thickness and projection type. However, the starting point was numerical calculations indicating the time of electrode travel (during the flow of current) must be significantly longer than in the case of the pneumatic system. In the welding technology, the profile of electrode travel was a preset parameter (similar to the parameter of force in the pneumatic system). During welding, the travel was performed according to a preset profile (without feedback).

The results obtained in the compu-

Table 8 — List of Characteristic Quantities Obtained in FEM Calculations

Projection Type C DX53 plate $g = 1.5$ mm $i = 10$ kA, DC current, $t = 60 + 240$ ms	Variant 1 0701c ($F = 110$ daN) pneumatic	Variant 2 0701b ($F = 220$ daN) pneumatic	Variant 3 0701d ($F = 440$ daN) pneumatic	Variant 5 1701d5 rate – value servo-mech.
1 Time for obtaining weld nugget $\phi = 6$ mm [ms]	129	172	—	182
2 Weld nugget diameter ϕ [mm] ($t_{weld} 300$ ms)	6.98	6.92	5.58	7.18
3 Weld nugget volume [mm ³] ($t_{weld} 300$ ms)	62.4	32.8	13.3	89
4 Energy [J] (total, after 300 ms)	2443	2036	1810	3421
5 Projection height reduction [mm]	0.98	0.97	0.99	0.98
6 Cold work	0.19	0.45	0.82	0.1
7 Max. power [kW] (momentary)	15.4	13.6	13.3	16.8
9 Energy [J] for obtaining nominal weld nugget diameter $\phi = 6$ mm	1229	1168	no weld nugget	2224
10 Weld nugget volume [mm ³] for nominal weld nugget diameter $\phi = 6$ mm	41	15	no weld nugget	64
11 Remarks	spatter	weld nugget is formed from outside (ring) inward, no spatter	weld nugget is formed from outside (ring) inward, overly small weld nugget diameter	proper weld nugget

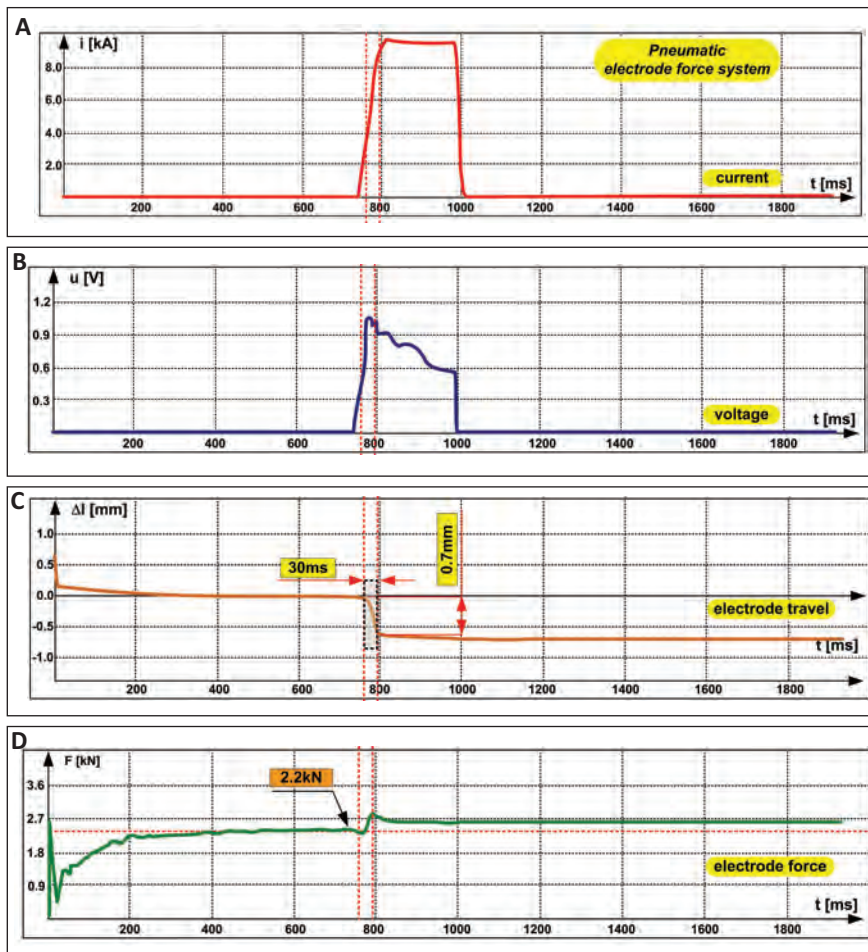


Fig. 12 — View of LogWeld measurement system monitor display with recorded waveforms of A — welding current; B— voltage; C— courses of electrode travel; D — electrode force for the pneumatic force system.

tational process were verified by technological welding tests, nondestructive examination (ultrasonic), and destructive examination (strength, peeling, and metallographic). Three technological welding tests were conducted for the pneumatic force system for the times of current flow 20, 40, 60, 80, and 100%; the servomechanical system for the times of current flow 1/4, 1/2, 3/4, 5/8, and 3/4 for metallographic tests; as well as measuring the selected characteristics of current, welding voltage, and energy supplied to the weld.

The metallographic tests involved the use of a 2% Nital reagent (etching time, 4 to 5 s).

Results

Presented are the results of the FEM calculations and experimental tests related to the analyzed process of

the projection welding of sheets for the two investigated (compared) electrode force systems (pneumatic and servomechanical).

FEM Calculations

The collected FEM calculation results include the following:

- 1) The temperature distribution in the welding area, illustrating the process of projection joint formation for selected times of welding current flow — Fig. 6.
- 2) The change of the projection height during welding — Fig. 7.
- 3) The course of dynamic resistance (the entire welding area) — Fig. 8.
- 4) The course of momentary power (the entire welding area) — Fig. 9.
- 5) The course of the weld nugget diameter growth — Fig. 10.
- 6) The course of an increase in the

weld nugget volume — Fig. 11.

All analyses were carried out for the pneumatic force system and, for comparison, the servomechanical force system — Figs. 6–11. In these images, t_{weld} is the time of welding current flow and i_{weld} is the value of welding current.

Figure 6 presents the results of the course of the projection weld formation along with the temperature distribution for various values of force exerted by the pneumatic system (Fig. 6A–D and by the servomechanical system, for comparison, Fig. 6E).

To compare the course of the process for various parameter settings, calculations were carried out for the maximum welding time of 300 ms or the calculations were finished when the weld nugget reached a nominal diameter of 6 mm.

Figure 7 presents a change in the projection height during welding. Part A represents the pneumatic force system, B shows the servomechanical force system (the solid line), and, for comparison, the pneumatic force system (dashed line). In the case of the pneumatic system, a change in the height of a projection (cold work) before the flow of welding current depends on the value of force and amounts to the following:

- 1) 0.19 mm (19%) for a 1.1-kN force.
- 2) 0.45 mm (45%) for a 2.2-kN force.
- 3) 0.82 mm (82%) for a 4.4-kN force.
- 4) 0.92 mm (92%) for a 5.5-kN force.

A further reduction of the projection height is affected by Joule heat during the flow of welding current. According to the calculations, in the case of the most favorable welding conditions (best welding conditions), for a force of 2.2 kN, the projection is completely crushed after a mere 20 ms. In turn, Fig. 7B presents the course of a decrease in the projection height for various values of force in the case of the pneumatic system (dashed line) and servomechanical system (solid line).

Graphic quantities, including the waveform of resistance and momentary power as well as the simulation of an increase in the weld nugget diameter and volume, were supplemented with additional characteristic quantities obtained during the computational process. Afterward, these quantities were used in the analysis of the results obtained in the simulation of projection welding. The results are presented Table 8.

The numerical calculations were verified experimentally. Presented are the results of these (experimental) tests performed for the pneumatic force system, best welding conditions (parameters in Table 6, line number 2), and servomechanical system (parameters in Table 7, line number 2).

Experimental Verification

The experiments involved measurements of the welding parameters, for example, the welding current and voltage, travel of electrode (the reduction of a projection height), and force registered for the pneumatic and servomechanical systems — Figs. 12, 13.

Figure 12 presents the process of projection welding for the pneumatic force system in the form of process characteristic parameters. Related courses and waveforms were recorded using the LogWeld 2 measurement system and included welding current and voltage, electrode travel, and electrode force.

The next part of the experimental results includes technological welding tests (metallographic examination) (Tables 9 and 10) confirming the numerical calculations presented in Fig. 6B and E. As mentioned previously, the experiments were carried out for various welding times (20, 40, 60, 80, and 100%) of the nominal welding current flow time for the pneumatic system and (%, %, %, %, %, and 100%) of the nominal welding current flow time for the servomechanical system.

The experimental tests were conducted for a welding current value lower than the value used in the FEM calculation. This was due to the fact that welding at high current values was accompanied by expulsion. As mentioned before, expulsion is disadvantageous as it may trigger the phenomenon of shunting during projection welding (Refs. 9, 12).

Discussion

Following is a discussion of the results, separately, for the numerical calculations and experimental tests.

FEM Calculations

In the case of the servomechanical

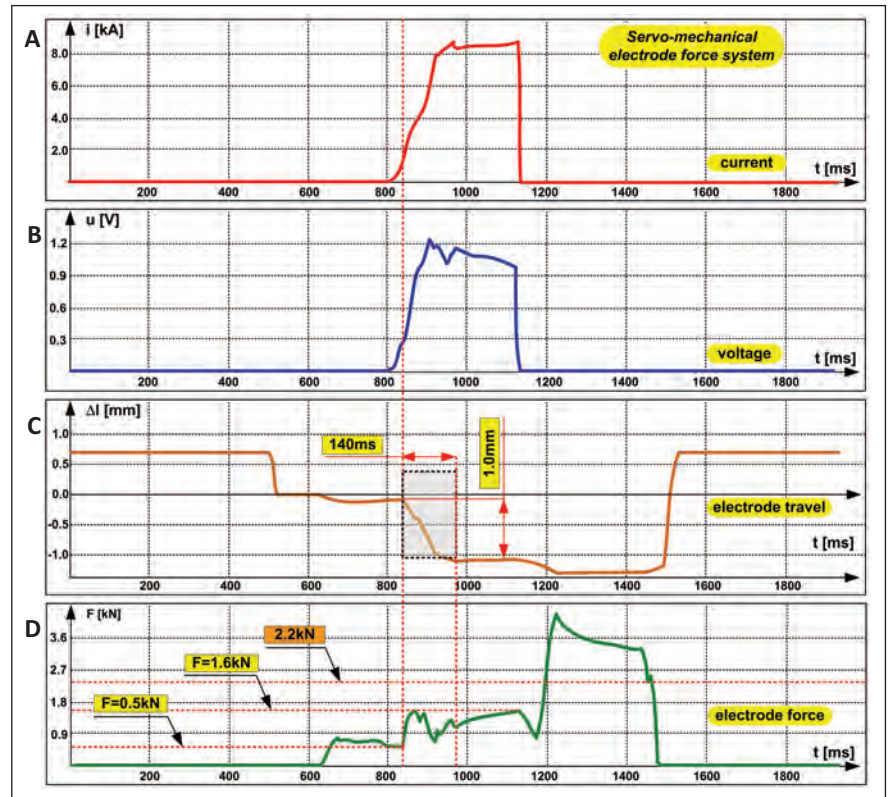


Fig. 13 — View of LogWeld measurement system monitor display with recorded waveforms of A — welding current; B — voltage; C — the courses of electrode travel; D — electrode force for the servomechanical force system.

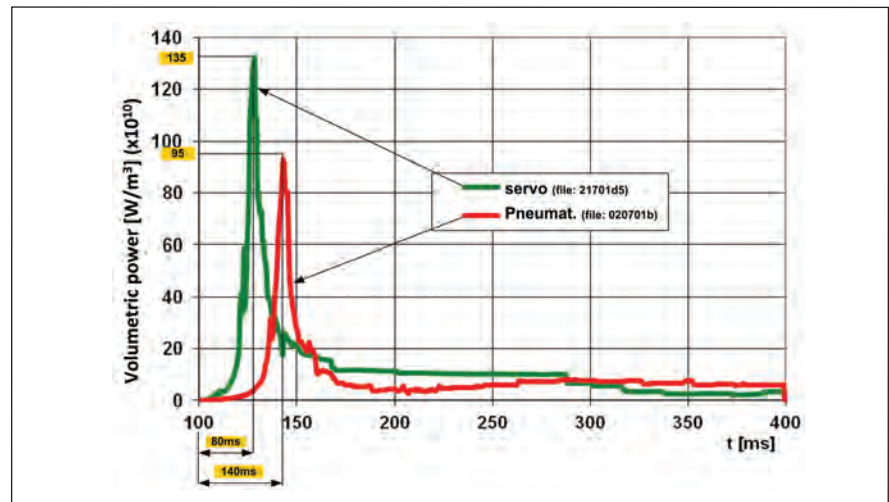


Fig. 14 — Distribution of the (volumetric) power density around point 866 (Fig. 1).

electrode force and travel system, it was possible to obtain a significantly longer time of the projection height reduction, i.e., 90 ms. In the case of the pneumatic force system, the projection height reduction time amounted to 20 ms (Fig. 7). These are the FEM calculation results in relation to the 80% projection height reduction. Similar results were confirmed in re-

lated experiments (20 ms for the pneumatic and 90 ms for the servomechanical system, Fig. 15) also in relation to the 80% projection height reduction.

In the experiments conducted, the time of the projection height reduction (100% of the height) amounted to 30 ms for the pneumatic force system (Fig. 15A) and 140 ms for the servo-

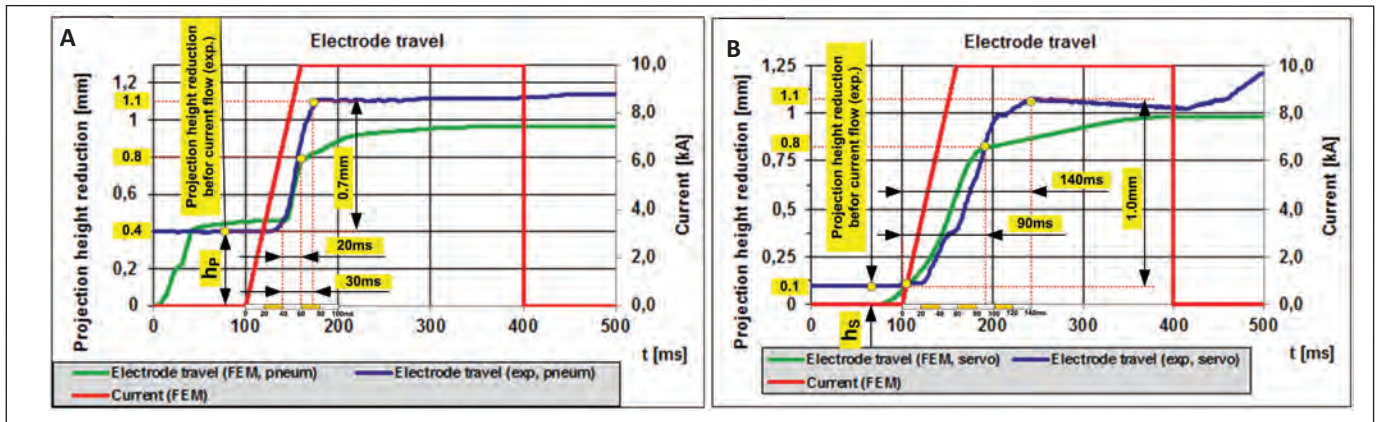


Fig. 15 — Courses of projection height reduction for FEM calculation and experiment. A — Pneumatic; B — servomechanical force system. Welding current is also present.

Table 9 — Comparison of Results of Metallographic Examination and FEM Calculations (pneumatic force system) for Various Current Flow Times (P = 2.2 kN)

Weld Time (%)	Left side: Metallographic structure of welded joint Right side: Temperature distribution (FEM calculations)	Remarks
20		Ring weld incomplete nugget
40		Ring weld incomplete nugget
60		Complete weld nugget φ nugget = 5.6 mm (FEM) 5.9 mm (metallography)
80		Complete weld nugget φ nugget = 6.1 mm (FEM) 6.0 mm (metallography)
100		Complete weld nugget φ nugget = 6.5 mm (FEM) 6.2 mm (metallography)

mechanical force system (Fig. 15B).

The initial projection height reduction amounted to 0.1 mm (10%). In the case of the pneumatic force system, for the best welding conditions (Fig. 6B), the projection height reduction amounted to 0.45 mm (45%) — Fig. 7. This value is 4.5 times lower and significantly more favorable than in the case of the best conditions in the case of the pneumatic system.

The advantages of the servomechanical systems are clearly visible. The lower force caused the higher (contact) resistance of the welding area (Fig. 8), and, consequently, the greater generation of power (Fig. 9) and energy (Table 8, variant 2, pneumatic system and variant 5, servomechanical system).

In the case of the servomechanical system, the formation (shape) of the weld nugget was similar as in the case of the minimum force exerted by the pneumatic system. This observation means the weld nugget was formed in the center (central part) and expanded outward.

More importantly, the phenomenon of liquid metal expulsion was not observed. This lack of expulsion could be ascribed to the manner in which the weld nugget expanded from the center outward.

Additionally, for the higher force (2.2 and 4.4 kN), it was possible to observe a phenomenon when a full nugget was formed from a ring nugget — Fig. 10. The central part of the future nugget was heated later than the outside area. A fully melted weld nugget was formed for a force of 2.2 kN and a current flow time of 120 ms

as well as for a force of 4.4 kN and a current flow time of 190 ms.

In the case of the servomechanical force system, the volume of a weld nugget was greater within the entire range of welding times, even if compared with the reduced force of 1.1 kN. This means the energy supplied to the weld was higher as well. This observation was confirmed by the higher welding power, especially at the end of the welding process, Fig. 9, and the entire energy supplied to the weld (Table 8).

Figure 14 presents the volumetric power density determined in the central place of the welding area, i.e., the cap of the projection, in the areas located near point number 886 — Fig. 1. The FEM computational program enabled the determination of the parameter of momentary power, but only for the whole welding area — Fig. 9. However, the determination of volumetric power density in a selected fragment of the whole welding area was important — Fig. 14.

The volumetric power density courses for the servomechanical and pneumatic electrode force system show differences in power generation (the nearest neighborhood of mesh point number 866). Due to the lower force, the projection height reduction at the beginning of the welding process was smaller (also due to the controlled process of the projection height reduction during the welding cycle); the servomechanical system caused the higher concentration of welding power (density) in the most favorable place, i.e., the projection cap. The said power was approximately 40% higher than in the case of the pneumatic system. In addition, in the case of the servomechanical system, the beginning of the fusion of the projection took place 40 ms earlier than in the case of the pneumatic system.

As can be seen previously, in the case of the servomechanical system, the initial time of material melting was approximately 43% shorter than the initial time of material melting in the case of the pneumatic system. Such a phenomenon was caused by a number of correlated factors and could be explained as described below. At the beginning, the projection height reduction before the flow of current was insignificant; therefore, the working area of the projection cap with the other material (the material being welded) was small.

As a result, the same welding current was accompanied by the favorably increased current density and concentration of energy, which, in turn, led to the higher temperature in the projection (particularly in the cap) and more favorable temperature distribution in the welding area (the cap material).

To illustrate the course within the whole welding range, calculations were carried out for the total welding time of 300 ms. Stars in the figures indicate the values of time when the weld nugget reached a diameter of 6 mm, i.e., when the process could be finished.

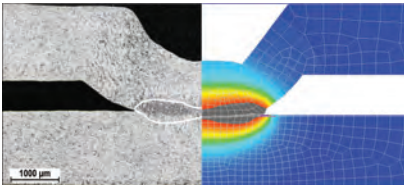
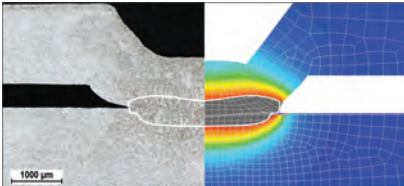
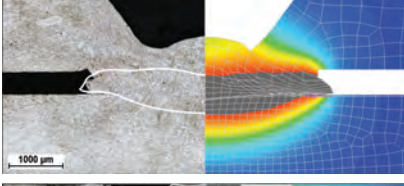
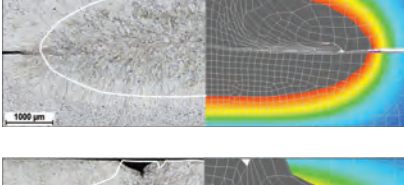
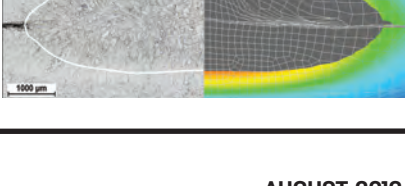
Experimentation

The presented results, in the form of

temperature distribution of the FEM calculations, and metallographic examination for the pneumatic (Table 9) and servomechanical force system (Table 10) reveal significant similarity as regarding to the course of the process.

For the pneumatic system (Table 9), the similarity mainly concerns the process of temperature distribution within the whole range of welding time. At the beginning, it is possible to observe the formation of a ring-shaped nugget (20 and 40% of the welding time), and next, the heating of the central part and formation of the complete weld nugget (60, 80, and 100% of the welding time). The results obtained in the form of the weld nugget diameter were satisfactory as they are restricted

Table 10 — Comparison of Results of Metallographic Examination and FEM Calculations (servomechanical force system) for Various Current Flow Times

Weld Time	Left side: Metallographic structure of welded joint Right side: Temperature distribution (FEM calculations)	Remarks
1/6		Complete weld nugget φ nugget = 2.1 mm (FEM) 1.8 mm (metallography)
2/6		Complete weld nugget φ nugget = 2.2 mm (FEM) 1.9 mm (metallography)
3/6		Complete weld nugget φ nugget = 3.9 mm (FEM) 3.2 mm (metallography)
5/6		Complete weld nugget φ nugget = 6.7 mm (FEM) 5.9 mm (metallography)"
6/6 (100%)		Complete weld nugget φ nugget = 6.8 mm (FEM) 5.8 mm (metallography)

within a $\pm 5\%$ tolerance range of the whole welding time analyzed.

In the case of the servomechanical system (Table 10), it is also possible to observe the similarity of the weld formation process. This similarity refers to the different manner of the weld nugget formation from the center outward. The differences of the FEM calculations and metallographic examination in relation to the weld nugget diameter were greater and, for the nominal value of 6 mm, amount to 12%.

Figure 15 presents the comparison of the projection height reduction obtained in the FEM calculations and projection height reduction obtained in the experiment in relation to the pneumatic and servomechanical system.

For the pneumatic force system (Fig. 15A), two courses of the projection height reduction (during the flow of current) are shown for the FEM calculations and experiment. During the experiment, the initial value of the cold projection height reduction (measured with a slide caliper in a separate experiment without current) amounted to 0.40 mm, and in the figure is designated as “ h_p ,” the value preceding the flow of current. Also, the projection height reduction was during the actual current flow.

It was possible to observe the similar time (30 ms) of the projection height reduction both in the experiment and calculation. The maximum value in the experiment was higher (connected with the deflection of electrode arms). The FEM model only includes the welding area composed of the electrodes and welded materials; the FEM model does not take into account the deflection of the electrodes.

For the servomechanical system (Fig. 15B), two courses of the projection height reduction (during the current flow) are shown for the FEM calculations and experiment. Before the flow of welding current, the projection height reduction was small (0.1 mm). Also, in this case, the reduction was measured with a slide caliper in a separate experiment without current. The low value of the projection height reduction is presented in Fig. 15B as the value “ h_s ,” preceding the flow of current. It can be seen the courses were similar. The maximum value in the ex-

periment was higher. This effect was also connected with the deflection of the electrodes.

The convergence of the results presented related to the distribution of the temperature in the welding area (Tables 9 and 10), and the courses of the electrode force and travel (Fig. 15) was satisfactory for both the pneumatic and servomechanical system.

Summarizing Comparison

The main advantage of the servomechanical system and its appropriate control (in comparison with the pneumatic system) is the possibility of controlling the travel of electrodes (the reduction of a projection height).

In the pneumatic system, the force of electrodes was controlled, and the travel of electrodes was the result of such control. This solution was not favorable due to the narrow window of welding parameters and the risk of the formation of an undesirable ring weld.

In the new solution (based on the servomechanical system), the travel of electrodes was a controlled parameter, and the force of electrodes was the result of such control.

The control of electrode travel (used in the servomechanical electrode force system) considerably changes not only the course of electrode force but also the welding process. The significant differences in the welding process were as follows: The minimum force of 0.5 kN (23%) (before the flow of current) is significantly lower than the force obtained using the pneumatic system (2.2 kN) (Fig. 13); the maximum force during projection welding was also significantly lower and amounts to 1.6 kN (73%) (Fig. 13); and the projection plasticization time is significantly longer (several times) in comparison to the projection plasticization time obtained using the pneumatic electrode force system — Fig. 15.

Such a change in the manner of the welding process control was desirable due to the following facts:

- 1) The projection contact area before the flow of current was smaller.
- 2) The density of current before the flow of current was higher.
- 3) The projection material melts in the most appropriate place (for example, the projection cap).

4) The weld was formed in the center and expands outward (an undesirable ring weld is not formed).

5) The power generated in the welding area (Fig. 9) is higher within the whole range of the welding time (the flow of current).

6) The energy supplied to the projection plasticization (during the flow of current) was 100% higher (according to the experiment, see Table 7).

Note that the reference parameter is the weld nugget with a diameter of 6 mm.

The results related to the higher energy supplied to the projection material (servomechanical system) were confirmed experimentally (see column F1 in Table 6, the pneumatic system, and Table 7, the servomechanical system).

Conclusions

The experimental tests verified and confirmed the advantageous character of the new solution involving the servomechanical electrode force system and its appropriate control. Therefore, it is justified to state the assumed objective of the research — the significant improvement of the projection welding process — was achieved.

The most important elements of the new process, dedicated to the projection welding of sheets with embossed projections and utilizing the servomechanical electrode force, were as follows:

1) The travel control (not force) of electrodes during the flow of welding current.

2) The exertion of a significantly lower force before the flow of welding current (the smaller cold projection height reduction) in comparison with the classical pneumatic electrode force system.

3) The extension of the welding current upslope time.

The control described makes it possible to obtain desirable welding power (density) space distribution. As a result, greater energy (density) was generated and concentrated in the projection material (at the beginning of a welding process taking place in the projection cap).

The new process uses the servomechanical force system and hybrid method of controlling the force and/or travel of electrodes. The hybrid method mentioned consists in controlling the force of electrodes before and after the flow of current as well as in controlling the travel of electrodes during the flow of current.

The most important is the control of electrode travel in a manner making it possible to extend the projection heating time, even several times, if compared with the classical pneumatic force system.

This article contains the results of research financed from funds provided by the Polish National Science Center and carried out within the project (N N501196940) performed by Instytut Spawalnictwa, the Wrocław University of Technology, and the Warsaw University of Technology in the years 2011–2013.

Acknowledgments

The research is continued within the framework of the TANGO project (TANGO1/267374/NCBR/2015) implemented in the years 2015–2017 and funded by the Polish National Science Centre and the Polish National Centre for Research and Development.

References

1. Mikno, Z. 2006. The monitoring of a resistance welding process as an opportunity for the improvement of quality and the reduction of welding costs. *Diagnostic Methods in Welding Engineering and Their Effect on the Quality of Joints and Welded Structures*. Instytut Spawalnictwa (Institute of Welding in Gliwice).
2. Larsson, J. 2008. Projection welding for nut and bolt attachment. *The Fabricator* (2).
3. Zhang, X., Chen, G., Zhang, Y., and Lai, H. 2009. Improvement of resistance spot weldability for dual-phase (DP600) steels using servo gun. *Journal of Materials Processing Technology*.
4. Tang, H., Hou, W., and Hu, S. 2002. Forging force in resistance spot welding. *Proceedings of the Institution of Mechanical Engineers, Part B: Journal of Engineering Manufacture*. 216, (7).
5. Gould, J. E. 2012. Joining aluminum sheet in the automotive industry — A 30 year history. *Welding Journal* 91(1): 23–34.
6. Agapiou, J. S., and Perry, T. A. 2013. Resistance mash welding for joining of copper conductors for electric motors. *Journal of Manufacturing Processes* 15(4): 549–557.
7. weldtechcorp.com/welding_concepts/projectionweld.html. Welding Technology Corp.
8. Sun, X. 2001. Effect of projection height on projection collapse and nugget formation — A finite element study. *Welding Journal* 80(9): 211-s to 216-s.
9. Mikno, Z., Bartnik, Z., Derlukiewicz, W., and Kowieski, Sz. 2013. Zgrzewanie garbowe w obliczeniach metodą elementów skończonych (projection welding in FEM calculations). *Przegląd Spawalnictwa* 11: 64–70.
10. Huang, H., and Tseng, K. 2009. Process parameters in resistance projection welding for optical transmission device package. *Journal of Materials Engineering and Performance* (6).
11. Mikno, Z., Bartnik, Z., Ambroziak, Z., and Pietras, A. 2012. Patent P. 401723. Sposób zgrzewania rezystancyjnego garbowego zwłaszcza blach stalowych z wytłoczonymi garbami (method for projection resistance welding of steel plates with embossed projections).
12. Mikno, Z., and Bartnik, Z. September 12–14, 2012. Projection welding with pneumatic and servomechanical electrode pressure system in FEM calculation — comparison. *The 7th International Seminar on Advances in Resistance Welding*. Busan, Korea.
13. Swantec, Inc., SORPAS® Software. Version 11.2. swantec.com.
14. Welding processes. *AWS Welding Handbook*, 9th edition, Vol. 3. Part 2, chapter 2, projection welding.
15. Gould, J. E. 1993. Projection welding. *ASM Handbook*, Vol. 6: Welding, brazing, and soldering, pp. 230–237. ASM International.
16. The database of the material and electrode parameters. Swantec, Inc., SORPAS® Software. Version 11.2.

Authors: Submit Research Papers Online

Peer review of research papers is now managed through an online system using Editorial Manager software. Papers can be submitted into the system directly from the *Welding Journal* page on the AWS website (aws.org) by clicking on “submit papers.” You can also access the new site directly at editorialmanager.com/wj/. Follow the instructions to register or log in. This online system streamlines the review process, and makes it easier to submit papers and track their progress. By publishing in the *Welding Journal*, more than 70,000 members will receive the results of your research.

Additionally, your full paper is posted on the American Welding Society website for FREE access around the globe. There are no page charges, and articles are published in full color. By far, the best people, at the least cost, will recognize your research when you publish in the world-respected *Welding Journal*.